

www.acsami.org Research Article

# Preparation of Efficient Ultraviolet-Protective Transparent Coating by Using a Titanium-Containing Hybrid Oligomer

Jiacheng Xing, Danhua Yuan, Hua Xie, Nan Wang, Hanbang Liu, Liping Yang, Yunpeng Xu,\* and Zhongmin Liu\*



Cite This: ACS Appl. Mater. Interfaces 2021, 13, 5592-5601



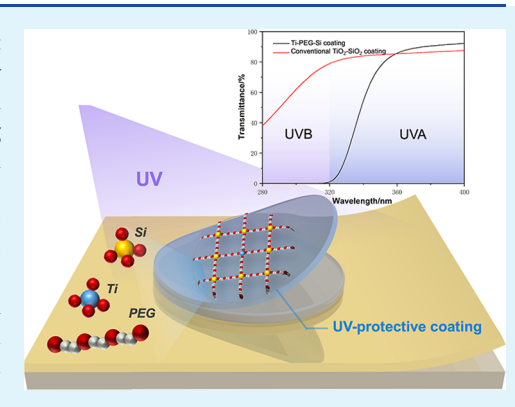
ACCESS

III Metrics & More

Article Recommendations

s Supporting Information

ABSTRACT: Ultraviolet (UV) radiation is closely related to people's lives, but excess UV exposure has led to a series of problems. UV protection technology plays a vital role in our life. The most commonly adopted UV protection technology is to use UV-absorbing materials to make protective coatings, including sunscreen cream for human skin and sunscreen coating for materials. Conventional organic UV-protective coatings have low stability and are sensitive to heat, while inorganic UV-protective coating with highly efficient UV-protective performance usually need high processing temperatures and exhibit low transparency. Here, we report a Ti-PEG-Si cross-linked inorganic—organic hybrid material, which exhibits good UV-absorbing performance. By using these UV-absorbing materials, an efficient transparent UV-absorbing coating could be easily prepared at room temperature (298 K). The UV-absorbing coating is mainly composed of titanium and silicon connected by PEG200. PEG200 as a cross-linker can improve the UV-absorption performance of the coating and increase its visible light transmittance.



At the same time, the existence of PEG200 can effectively increase the stability and elasticity of the coating and maintain its mechanical properties after UV irradiation. Furthermore, the coating could maintain highly UV-protective performance and could be transparent even after thermal treatment at high temperature (973 K). From this point of view, the hybrid materials have considerable application potential in next-generation UV protective coatings, especially with their utilization in heat-sensitive substrates or under high-temperature conditions.

KEYWORDS: UV-protective coating, titanium, UV-blocking materials, hybrid oligomer, transparent film, hydrolysis-resistant

#### **■** INTRODUCTION

Ultraviolet (UV) light plays an indispensable role in different areas of life and provides energy for all living creatures. <sup>1,2</sup> Conversely, UV light can also cause huge damage to humans and materials. <sup>3,4</sup> UV radiation is responsible for the discoloration, decomposition, and degradation of plastics, dyes, paintings, etc. <sup>1,5,6</sup> The ultraviolet radiation b band (UVB, 280–310 nm) in UV light typically causes sunburn and direct DNA damage via pyrimidine dimer formation, and the ultraviolet radiation a band (UVA, 320–400 nm) causes suntan; thus, UV radiation plays a direct role in photocarcinogenesis. <sup>7–9</sup>

At present, commonly used UV absorbers are mainly divided into two categories. <sup>10,11</sup> Organic UV-absorbing molecules usually include a phenol functional group that converts the energy of UV radiation into thermal energy, such as octocrylene and oxybenzone. <sup>12–14</sup> However, these aromatic compounds have low stability and are sensitive to heat, which greatly reduce their lifetime when used under high-temperature conditions. <sup>15,16</sup> Moreover, organic UV absorbers require additional dispersant and stabilizer systems. <sup>10,17</sup> Another alternative is inorganic UV absorbers, which are mainly

based on titanium dioxide and zinc oxide nanoparticles.<sup>18–20</sup> These materials have good thermal stability, but their transparency in the visible region is low due to their high reflectivity of light, making them difficult to apply in optical devices.<sup>21,22</sup> In addition, the formation of inorganic UV-absorber coatings with highly efficient UV-protective performance usually requires high temperatures, which is also difficult to apply with heat-sensitive materials.<sup>23–25</sup> Titanium sources such as titanium tetrachloride and titanates, which are usually used as precursors to prepare inorganic UV-protective coatings, are very easily hydrolyzed, and it is difficult to control the uniformity of the product.<sup>26,27</sup>

Therefore, great efforts have been devoted to developing novel UV absorbers and avoiding the above shortcomings. <sup>28–36</sup> In the early 2000s, some researchers began to focus on

Received: November 23, 2020 Accepted: January 12, 2021 Published: January 21, 2021





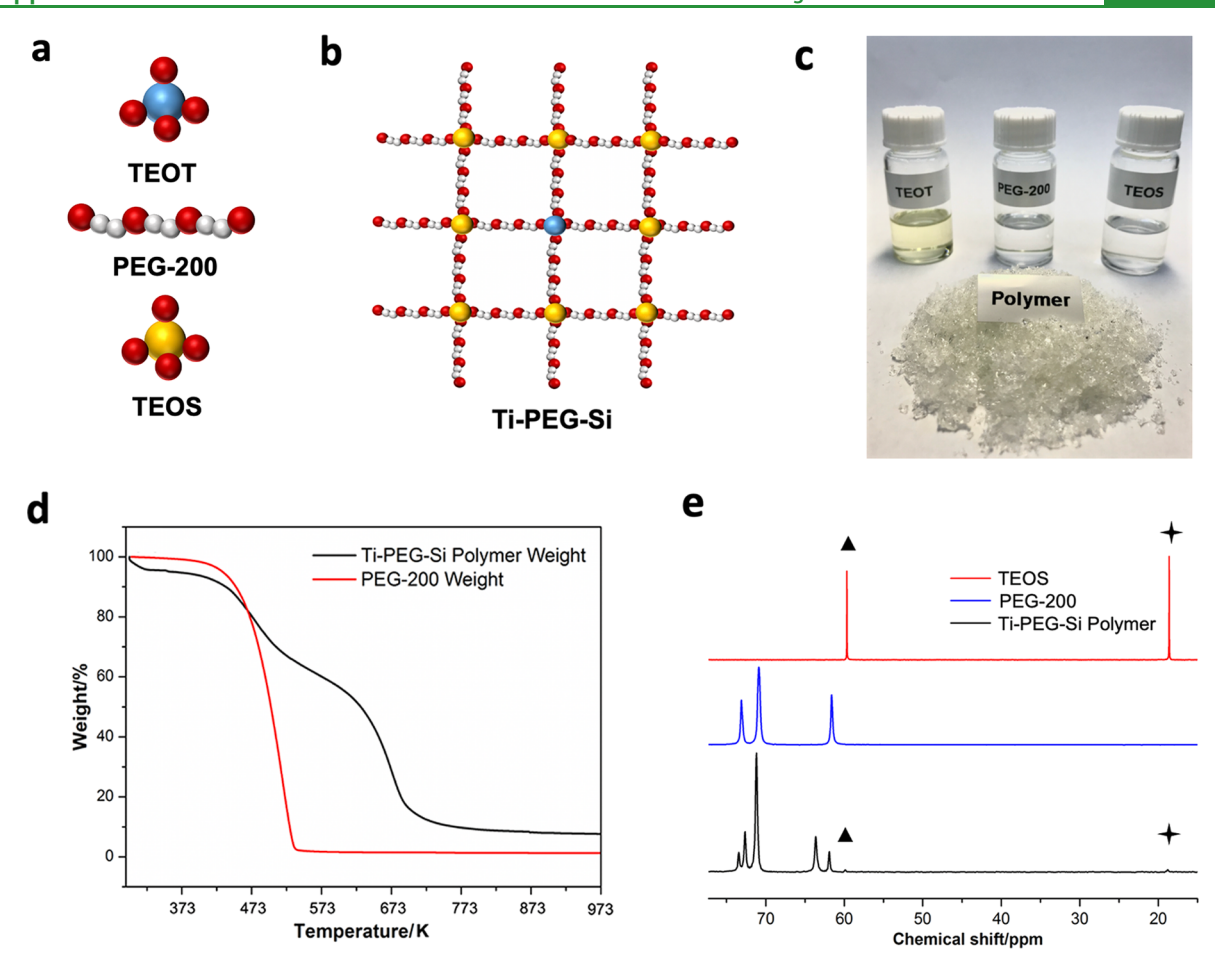


**Figure 1.** (a) Structure of the precursors and (b) Ti-PEG-Si UV absorbers. Gray: C, red: O, yellow: Si, and blue: Ti. (c) Photos of the raw liquid materials and solid UV absorber product. (d) TGA analysis and (e) <sup>13</sup>C MAS NMR of the Ti-PEG-Si UV absorber.

entrapping UV absorbers in a sol-gel-derived ormosil matrix. 3,37-40 The resulting coatings present high stability and strong absorption in the UV region of the spectrum. However, these coatings suffer from leaching problems. 15 Therefore, highly effective titanium-containing materials have attracted our attention. Although traditional organic titanium materials are easy to coat, they have poor stability and are easily hydrolyzed and whitened. 26,41 Conversely, inorganic titanium materials have high stability, but they usually need a high treatment temperature and have low transparency in the visible region; furthermore, they do not easily form into a film for coating on the surface of a material. 35,42,43 In order to overcome the shortcomings of conventional titanium-containing materials, many investigators have made great efforts. 44-48 Bi et al. designed a modified titanium dioxide@graphene oxide/poly(vinyl alcohol) nanocomposite to obtain UV resistance. 44 Guo et al. reported a facile bottom-up fabrication process to prepare a transparent TiO<sub>2</sub>/Ce xerogel coating for natural engineering materials.<sup>45</sup> In this work, we try to find a titanium-containing UV absorber with high stability that easily forms a coating while maintaining high transparency in the visible region.

## ■ RESULTS AND DISCUSSION

In this work, we synthesize a Ti-Si cross-linked inorganic—organic hybrid material, which easily forms an efficient UV-absorbing coating at room temperature (298 K) and also has highly UV-protective properties even after thermal treatment

at 973 K. The thickness of the coatings is controllable, and the coating remains transparent for more than 1 year. The Ti-Si cross-linked coatings show very strong UV absorption, especially in the wavelength range where UV damage is greatest (290-350 nm). At the same time, the Ti-Si crosslinked coating has high transparency and less absorption in the visible region. The Ti-Si cross-linked inorganic-organic hybrid materials solve the problems that traditional titaniumcontaining materials suffer from, such as being easily hydrolyzed and losing transparency in the visible region. The Ti-PEG-Si cross-linked hybrid UV absorber is synthesized by using tetraethyl titanate (TEOT), tetraethyl orthosilicate (TEOS), and polyethylene glycol (PEG200) as the reactants through transesterification reactions, as shown in Figure 1a and Figure S1. The product obtained was named Ti-PEG-Si. During the transesterification reactions, TEOT serves as both the reactant and the catalyst. The ratio of silicon to titanium in the UV absorber is adjustable.

After the transesterification reactions, the alkoxy groups of TEOT or TEOS were transesterified with PEG200 to form a network-like polymerized compound (Figure 1b). The photos show that the liquid raw materials were successfully transformed into transparent solid products (Figure 1c). The resulting UV absorber generally has a polymerization degree of 10 (see more information in the Experimental Section and Supporting Information). The thermogravimetric analysis (TGA) and <sup>13</sup>C MAS NMR analysis of the UV absorber are shown in Figure 1d,e. TGA analysis showed that PEG200,

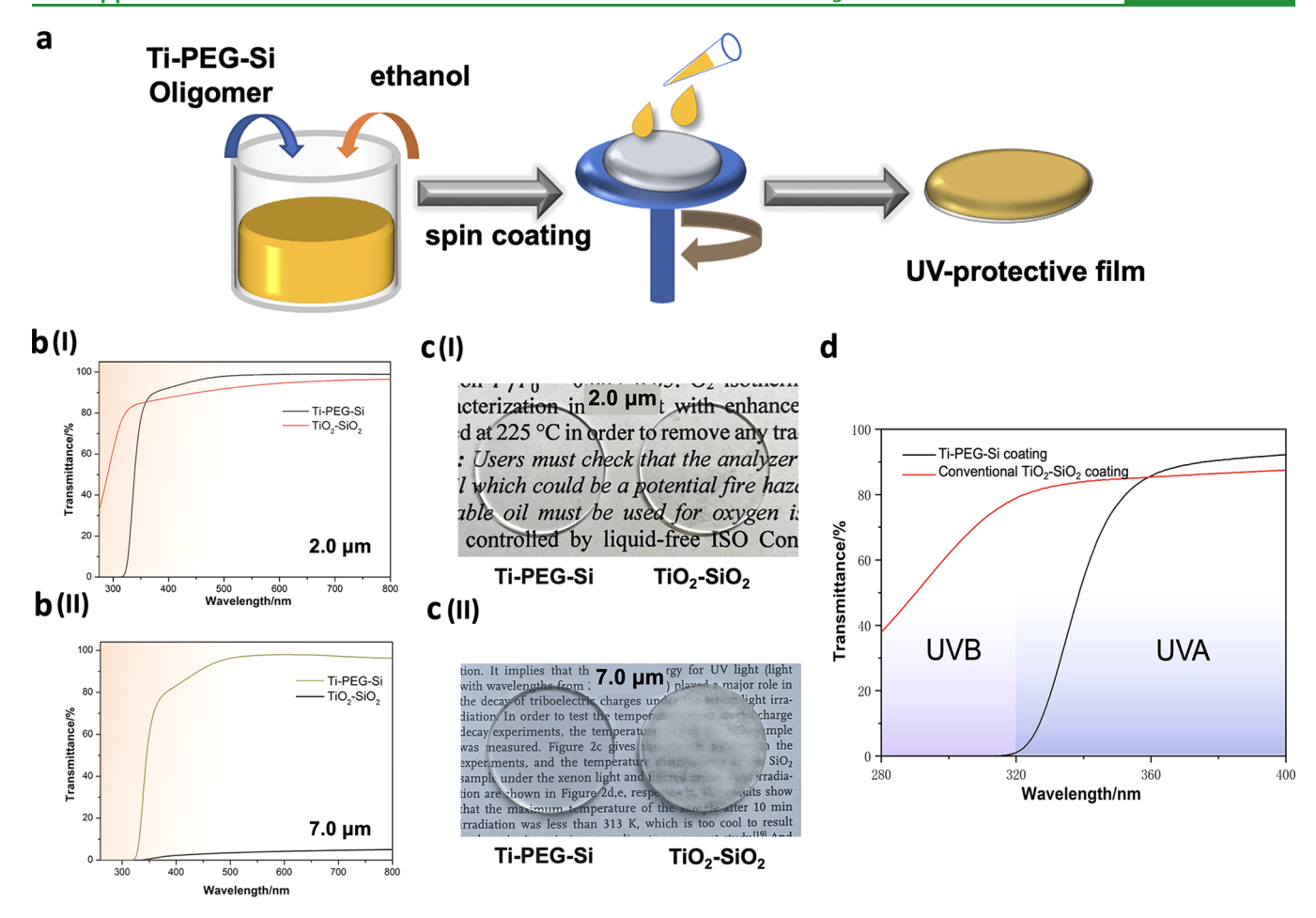


Figure 2. (a) Preparation of the UV-absorbing coatings by spin-coating. (b) UV-visible transmittance spectra of the Ti-PEG-Si coatings and TiO<sub>2</sub>-SiO<sub>2</sub> coatings with the same thickness of (I) 2.0  $\mu$ m and (II) 7.0  $\mu$ m. (c) Photo of the Ti-PEG-Si coatings (left) and TiO<sub>2</sub>-SiO<sub>2</sub> coatings (right) with the same thickness of (I) 2.0  $\mu$ m and (II) 7.0  $\mu$ m. (d) UV-visible transmittance spectra of the Ti-PEG-Si coatings and TiO<sub>2</sub>-SiO<sub>2</sub> coatings with the same thickness of 2.0  $\mu$ m in the region between 280 and 400 nm.

which is one of the raw materials, decomposed at 473 K, and there were two distinct weight loss peaks in the Ti-PEG-Si UV absorber. This was mainly because a small part of PEG200 did not participate in the polymerization; thus, the polymer slightly decomposed at 473 K. At 653 K, the UV absorber significantly decomposed.

It is worth mentioning that there is a slight weight loss at 323 K, which is mainly due to the fact that a small amount of ethanol generated in the polymerization process is not completely removed after synthesis. The <sup>13</sup>C MAS NMR analysis showed that the peaks from the methylene and methyl groups on the silicon ester and the titanium ester were significantly weakened and lowered at 58.2 and 18.2 ppm, respectively, which proved that the ethyl groups of the original tetraethyl orthosilicate and tetraethyl titanate were removed during the transesterification reactions. The Ti-PEG-Si UV absorber had good ethanol solubility. In addition, it is worth noting that the Ti-PEG-Si UV absorber has a very high resistance to hydrolysis, and its aqueous solution and coatings can remain clear and stable after more than 1 year at room temperature (298 K), as shown in Figure S2. However, the raw materials of TEOT and TEOS are very easily hydrolyzed even in a moist environment. Organic titanium materials are easily hydrolyzed, and inorganic titanium materials lose transparency in the visible region. From this point of view, a hydrolysisresistant and transparent Ti-PEG-Si polymer should be an ideal UV absorber for different substrates.

In this work, a Ti-PEG-Si inorganic—organic hybrid UV-absorbing coating was prepared by spin-coating (Figure 2a). The synthesized UV absorbers were dissolved in ethanol and added to the substrates with the sample holder spinning at different revolutions per minute. The quartz glass substrates were highly transparent in the UV and visible regions. After the spin-coating treatment, the obtained coatings were dried at room temperature (298 K) for 1 day or at 333 K for 2 h. In addition, these two drying methods have no obvious effect on the properties of the coating, as shown in Figure S11. To verify that the UV-protective coatings still have UV absorption properties under high-temperature conditions, the coatings were calcined at 973 K. The experimental details are provided in the Experimental Section.

To take advantage of the best UV-adsorption performance of the coating, the titanium content of the Ti-Si cross-linked hybrid UV absorber was investigated. As shown in Figure S5, UV absorbers with a Ti content of 20% (n(Si/Ti) = 4, 2.12 wt%) had a very strong absorption in the whole UV region and showed high transparency in the visible region. Therefore, UV absorbers with a Ti content of 20% (n(Si/Ti) = 4, 2.12 wt%) were selected to investigate the features of the Ti-Si cross-linked hybrid UV absorber. We prepared TiO<sub>2</sub>-SiO<sub>2</sub> coatings with the same 7.0 and 2.0  $\mu$ m thicknesses as the Ti-Si cross-

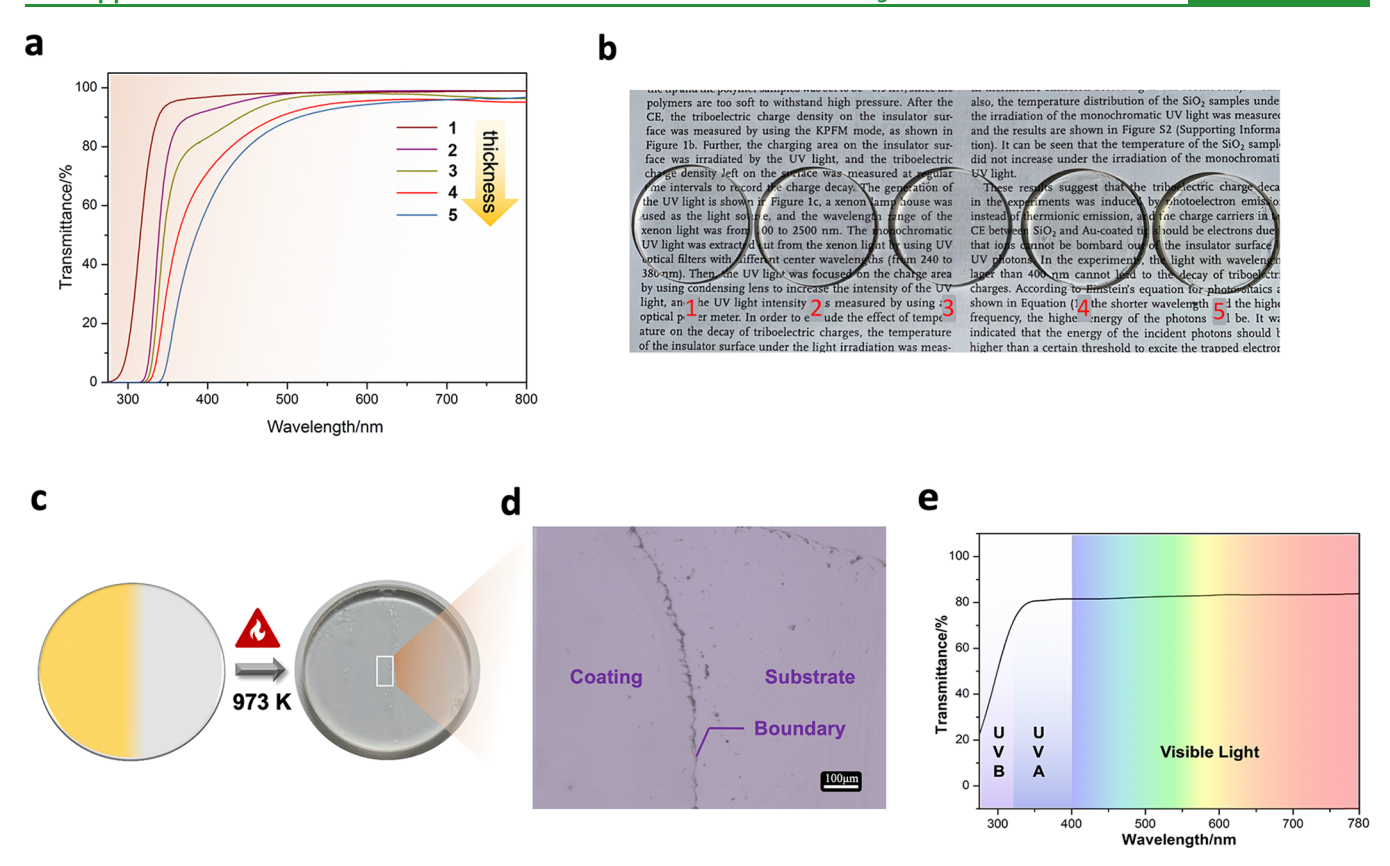


Figure 3. (a) UV–visible transmittance spectra of the Ti-PEG-Si coatings with different thicknesses: (1) 0.1 μm, (2) 2.0 μm, (3) 7.0 μm, (4) 15.0 μm, and (5) 88.0 μm. (b) Photo of the Ti-PEG-Si coatings: (1) 0.1 μm, (2) 2.0 μm, (3) 7.0 μm, (4) 15.0 μm, and (5) 88.0 μm. (c) The Ti-PEG-Si coatings treated under 973 K. (d) Optical microscopy images of the edge of the high temperature-treated coatings. (e) UV–visible transmittance spectra of the Ti-PEG-Si coatings after high-temperature treatment.

linked hybrid UV protective coating by using a sol-gel method at room temperature (298 K). Additionally, the titanium weight content of the hybrid coating is the same with the conventional TiO2-SiO2 coating. The difference in UV absorption between the oxidized coating and our synthetic inorganic-organic hybrid UV-absorber coating is shown in Figure 2b,c. For the TiO<sub>2</sub>-SiO<sub>2</sub> coating with a thickness of 2.0  $\mu$ m, the oxide coatings and inorganic-organic hybrid UVabsorber coatings gave slightly different transmittances in the visible range (400-700 nm, Figure 2b(I)). The transmission rate of the TiO<sub>2</sub>-SiO<sub>2</sub> coatings in the visible range is lower than that of the inorganic-organic hybrid UV-absorber coatings because their high degree of crystallinity refracts the light. The difference in the transmittance spectra of the UV region between the two coatings is large. The transmission spectrum shows that the inorganic-organic hybrid UV-absorber coating has a much lower transmittance in the UV region than that of the TiO<sub>2</sub>-SiO<sub>2</sub> coatings. In the range of 320-350 nm, the transmittance of the inorganic-organic hybrid UV-absorber coating is significantly reduced, and the transmittance rate at 320 nm reached 0, while the TiO<sub>2</sub>-SiO<sub>2</sub> coatings have a transmittance rate of 78.9% at 320 nm, as shown in Figure 2d. The above results suggest that the inorganic-organic hybrid UV-absorber coatings have a very strong absorption in the UV region and can effectively prevent substrates from being damaged by UV rays, especially substrates made from heatsensitive materials. It can be clearly seen that the 7.0  $\mu$ m TiO<sub>2</sub>-SiO<sub>2</sub> coatings exhibit a distinct white color and their light transmission in the visible region is significantly reduced in

Figure 2b(II),c(II). This oxide coating is not suitable for situations requiring high transparency, such as artwork and precision optics instruments. At the same thickness of 7.0  $\mu$ m, the inorganic—organic hybrid UV-absorber coatings maintain high transmission in the visible region, a wavelength range of 400–780 nm, and the transmission in the UV region is very low, especially in the region where the most damage was caused by UV rays (290–350 nm). Additionally, there was no transmittance of UV rays below a wavelength of 328 nm (Figure 2b(II)). This is mainly attributed to the incorporation of titanium in the network of the Ti-Si cross-linked hybrid UV absorber.

Through the above analysis, it was found that the inorganic organic hybrid UV-absorber coatings strongly absorbed UV light, so we further investigated the effect of coating thickness on the UV absorption performance (Figure 3a,b). As the thickness of the UV-absorbing coating increased, its UVabsorbing ability gradually increased. When the thickness of the coating was between 0.1 and 15.0  $\mu$ m, the UV absorption coating had a higher transmittance in the visible range of the spectrum (400-700 nm). When the thickness was increased to 88.0  $\mu$ m, the transmittance in the visible range decreased, but the UV absorption performance had a large improvement. In the preparation of the UV-absorbing coatings above, they were all treated at 333 K or room temperature (298 K) to form a UV-absorbing coating. This proves that this method is very suitable for the UV protection of substrates that are sensitive to heat, such as plastic or some dyes. However, there are also some cases where the substrates need to be treated at high

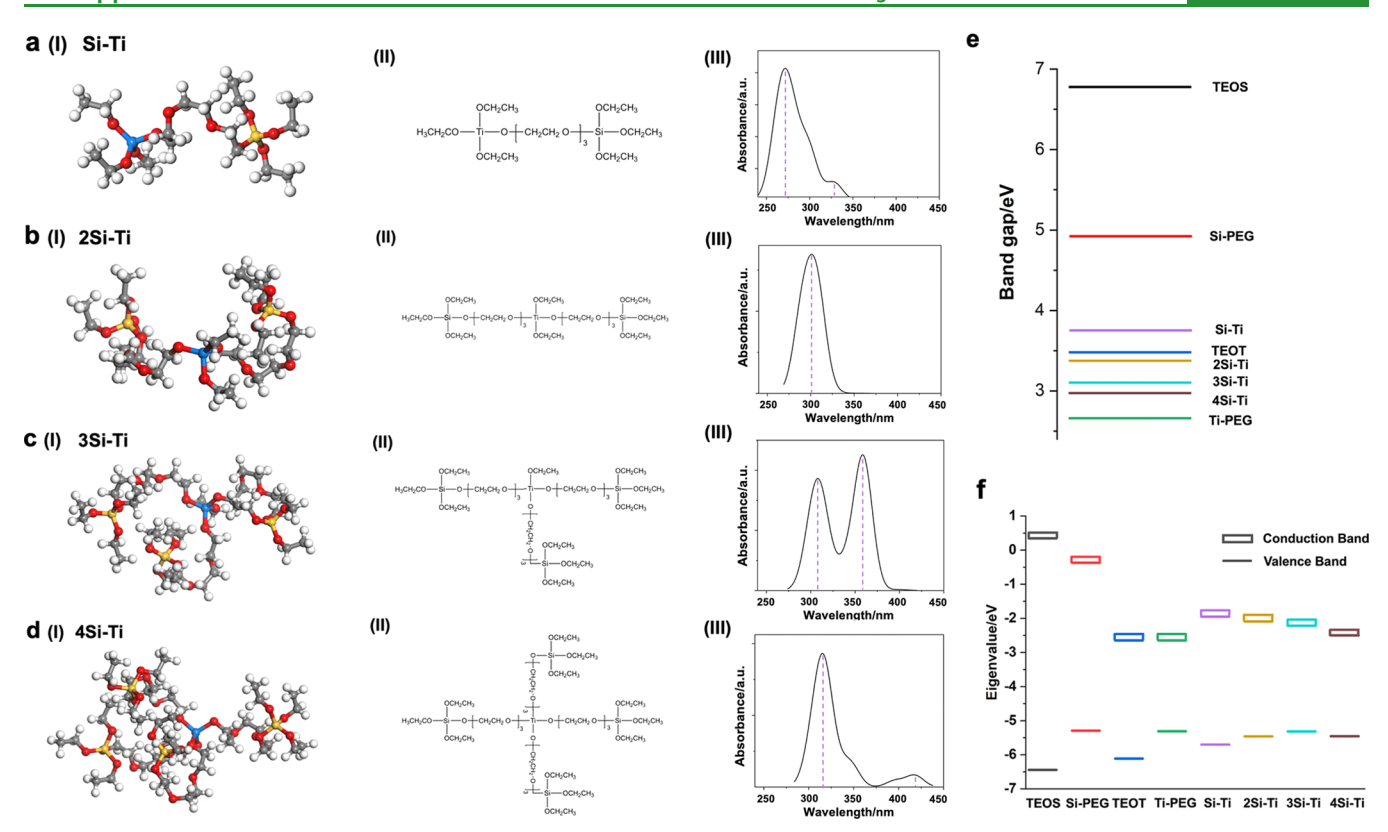


Figure 4. Simulation of the UV absorbers. (a-d, I, II) UV absorbers with different atoms used for theoretical calculation. White: H, dark gray: C, red: O, yellow: Si, and blue: Ti. The system contained one silicon and one titanium atom named as Si-Ti and so on. (a-d, III) TD-DFT electronic excitation spectra of the Ti-PEG-Si UV absorber. (e) Predicted band gap of the different titanium and silicon-containing materials. (f) Calculated valence band and conduction band energies of different titanium and silicon-containing materials.

temperature. Therefore, a test was conducted on whether the coatings could still effectively absorb UV rays if the temperature reached the decomposition temperature of the inorganic-organic hybrid UV absorber. To determine this, the abovementioned UV absorbing coatings were treated at higher temperatures, such as 973 K (Figure 3c). After calcination, we find that the resulting UV-absorbing coating remains transparent and has a thickness of approximately 53 nm with a relatively regular boundary (Figure 3d). It still maintains a certain absorption in the UV region (Figure 3e), especially in the range where the damage caused by UV rays is most severe (290-350 nm). However, compared with that of the UV absorbing coatings formed at room temperature (298 K) or 333 K, the efficiency of the absorption is significantly reduced, and it is relatively close to that of the TiO2-SiO2 oxide coating synthesized by a conventional sol-gel method. It can be seen from the thermogravimetric curve (Figure 1d) that, when the treatment temperature is 653 K, there is an obvious weight loss peak, which is mainly due to the decomposition of PEG200 in the hybrid material. Therefore, at 973 K, the organic compounds in the hybrid materials completely decomposed. At this time, inorganic TiO2 and SiO2 remained in the UV absorption coating. This process is very similar to the preparation of inorganic  $TiO_2$ - $M_xO_y$  (M = Si, Ce, Pb, etc.) coatings by traditional methods.<sup>49</sup> In the traditional method, the organic titanium source is usually dissolved in the aqueous solution of alcohols, and the sol is prepared in relatively lowtemperature aging. Then, the sol is coated on the substrate and calcined at a higher temperature, such as 773 K, to obtain the inorganic titanium-containing UV absorption coating.<sup>50</sup>

Similarly, this inorganic—organic hybrid UV absorber could form an inorganic  ${\rm TiO_2\text{-}SiO_2}$  coating at high temperature, so it can still maintain a certain UV absorption capacity. Thus, the inorganic—organic hybrid UV absorber can not only form a UV absorbing coating at room temperature (298 K) but also provide UV protection at a higher temperature. This also greatly expands the application of this inorganic—organic hybrid UV absorber, which can be used for efficient UV protection in heat-sensitive substrates or under high-temperature conditions.

The optical absorption properties of the hybrid UV absorbers were also investigated by means of time-dependent density functional theory (TDDFT) calculations. 51-54 Oligomers with different silicon content were selected for analysis by this theoretical method. The ethoxyl group on the titanium ester was gradually replaced by Si-PEG fragments, as shown in Figure 4a-d. The time-dependent DFT excitation spectra (Figure 4-III) showed that all the hybrid UV absorbers had a strong absorption in the range of the UV region. Comparing the simulated absorption spectra with the increase of the substitution degree of the ethoxyl group on titanium by the Si-PEG fragment, there was a red shift from Si-Ti (Figure 4a) to 4Si-Ti (Figure 4d). This phenomenon was mainly attributed to the increasingly electron-donating group, PEG200, moderately decreasing the band gap from 3.8 to 3.0 eV (Figure 4e,f). 55 Additionally, we extended the computational exploration to TEOS and TEOT and replaced all the ethoxyls on TEOS and TEOT by PEG200 (Si-PEG and Ti-PEG). Our calculations predicted that Si-PEG and Ti-PEG would exhibit a larger red shift than traditional TEOS and

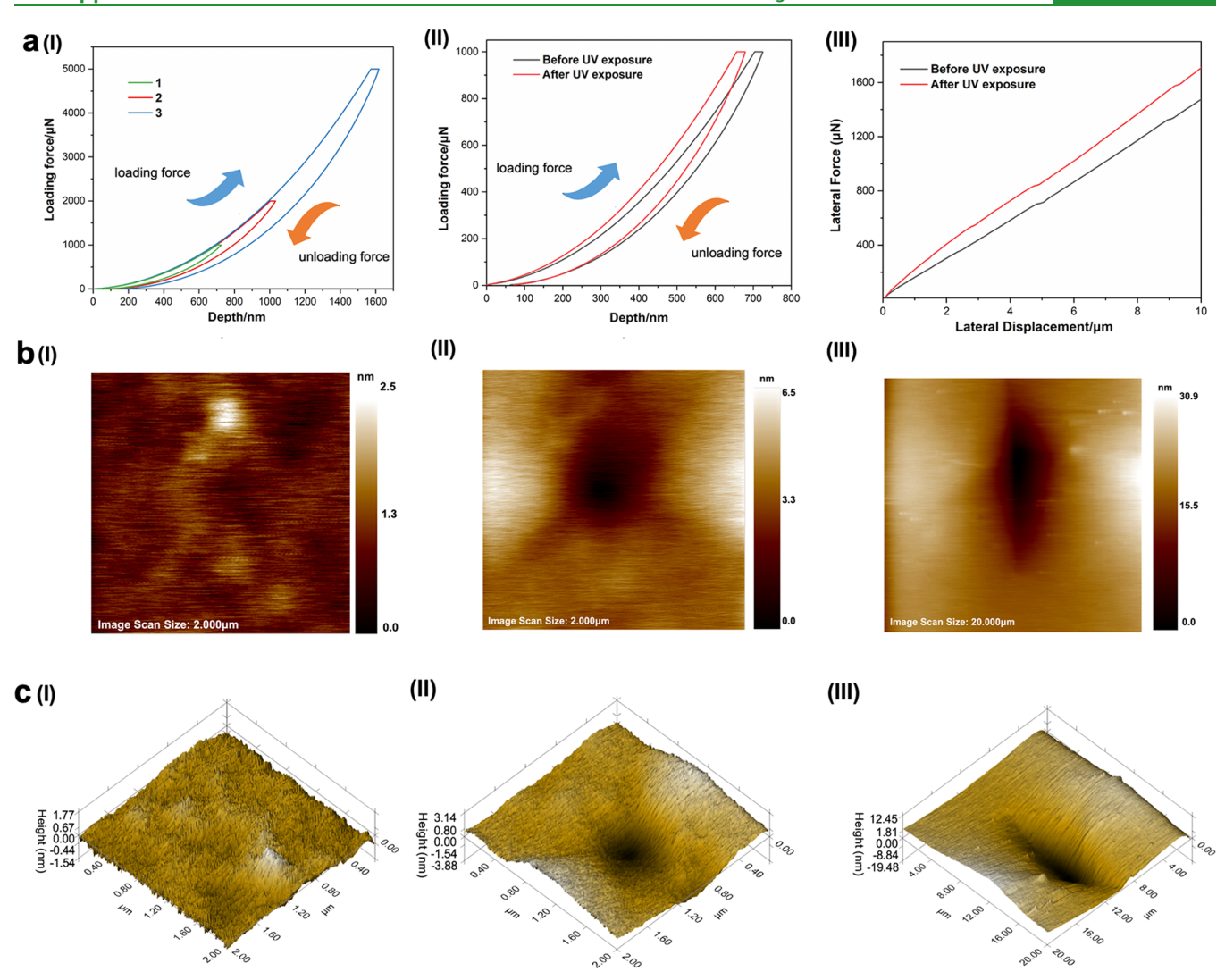


Figure 5. Mechanical performance of the UV protective coatings. (a) (I) Nano-indentation experiment of the coatings with different loading forces. (1)  $1000 \mu N$ , (2)  $2000 \mu N$ , and (3)  $5000 \mu N$ . (II) Nano-indentation experiment of the coatings before and after UV exposure. (III) Scratch test results of the coatings before and after UV exposure. (b, c) Two-dimensional (2D) and three-dimensional (3D) scanning graphs of surface topography: (I) original UV-protective coating, (II) the coating after a loading force of  $5000 \mu N$  by the probe, and (III) the coating after the scratch test with a longitudinal loading force of  $8000 \mu N$ .

TEOT, mainly due to the increase in electronic density of PEG200. The band gaps of TEOS and TEOT were 6.8 and 3.5 eV, while those of Si-PEG and Ti-PEG were 4.9 and 2.7 eV, respectively (Figure 4e,f). The simulated and experimental transmittance rates of the UV absorbers are shown in Figure S8. The simulated transmission spectra of the hybrid UV absorbers were relatively in good agreement with the experimental spectra. The reason for this difference was that the UV absorbers synthesized in the experiment was the mixture of a various degrees of polymerization. Based on the above theoretical method, the origin of the UV absorption may be attributed to the Ti-PEG-Si like structure of the UV absorber

The mechanical properties of the UV-protective coating were characterized and evaluated by nano-indentation. In the experiment, a coating thickness of 2.0  $\mu$ m on quartz slide was selected for testing. During the nano-indentation test, the probe applied different loading forces. When the loading force was 5000, 2000, and 1000  $\mu$ N, respectively, the indentation test diagram was obtained and displayed in Figure 5a-I. The depth of the probe pressing into the coating increases with the

increase of the loading force. When a different loading force is applied, the deformation degree of the coating is equivalent, that is, the loading force curves are highly coincident. When the maximum loading force reaches 5000  $\mu$ N, the depth of the coating is 1.5  $\mu$ m. At the same time, it can be seen from the loading force curves that the coating is not cracked during the nano-indentation test. With the removal of the loading force, the elastic deformation of the coating can be seen in the curve. When the loading force of the probe is removed, the coating can be recovered again. The surface topography measured by the probe is shown in Figure 5b-I,c-I. The surface of the prepared UV protective coating is relatively smooth and flat. The change of the surface depth is only within 2.5 nm. Figure 5b-II,c-II are the scanning graphs of the coating after a force of 5000  $\mu$ N is applied by the probe. When the force is unloaded, only an indentation with a depth of approximately 6 nm is left on the surface. It also proves that the elasticity of the coating is good. The nano-indentation hardness of the coating is approximately 0.13 GPa, and the reduced elastic modulus is 1.03 GPa. In order to verify whether the mechanical properties of the coating have changed after UV irradiation, we have

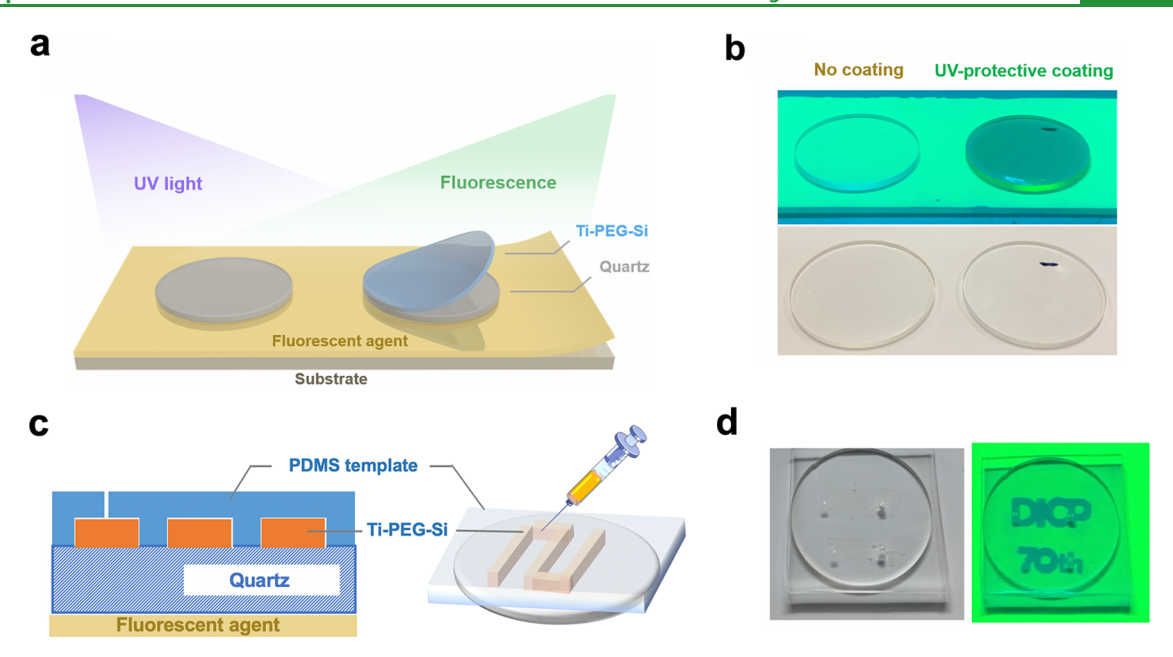


Figure 6. Application of the UV-protective coating. (a) Quartz with UV-protective coatings  $(2.0 \, \mu \text{m})$  and an uncoated one placed on the surface of the plate. The plate with a fluorescent agent can generate fluorescence under UV light. (b) The quartz slides with a UV-protective coating and without a coating were tested under UV light (top). Slide placed on the plate without UV light (down). (c) PDMS chips with UV absorbers injected inside and contacted with a quartz slide. (d) PDMS chips placed on the surface of the plate, which can generate fluorescence under UV light and show the channels of the chips.

tested the nano-indentation of the coating before and after UV irradiation of 15 h. As shown in Figure 5a-II, it can be seen from the loading force curve that the mechanical properties of the coating do not change significantly before and after UV irradiation. After UV irradiation, the hardness of the coating increases to 0.14 GPa, the reduced elastic modulus is 1.20 GPa, and the elasticity is slightly weakened. At the same time, the scratch test results of the coating before and after UV irradiation are shown in Figure 5a-III. The longitudinal force from 0 to 8000  $\mu N$  is gradually increasing when the probe applies to the coating with a scratch distance of 10  $\mu$ m. With the increase of the scratch depth, the lateral force increases correspondingly. When the longitudinal loading force of the nano scratch probe is 8000  $\mu$ N, the maximum value of the lateral force is approximately 1700  $\mu$ N. It can also be seen from the scratch curve that, even when the longitudinal loading force reaches 8000  $\mu$ N, the coating can still maintain good mechanical properties without cracking. It can be observed from Figure 5b-III,c-III that, at the end of the scratch test, only a shallow scratch with a depth of approximately 30 nm appeared on the coating surface. The length of the scratch exceeds 10  $\mu$ m past the probe, as shown in Figure 5b-III. This is because the probe cannot immediately unload the 8000  $\mu$ N loading force at the end of the scratch test. Through the above nano-indentation and scratch experiments, the UV-protective coatings show good mechanical properties and stability. It can also be verified that the coating can maintain the stability of its mechanical properties after UV irradiation.

To demonstrate the performance of the UV-absorbing coating, we conducted experiments on UV protection. A quartz glass with the inorganic—organic hybrid UV-absorber coating (2.0  $\mu$ m) and an uncoated quartz glass are placed on the surface of a plate that can generate fluorescence under UV excitation. The quartz glass substrates are highly transparent in the UV and visible regions. The quartz slides with and without a coating both show higher transparency in the absence of UV

light, but a significant difference is observed under UV light. The coated substrates absorb the UV light completely, so the back plate cannot fluoresce under the excitation of UV rays, showing a grayish black color; conversely, the uncoated quartz substrate can completely transmit ultraviolet rays, and the excited plate generates fluorescence (Figure 6a,b). Furthermore, a series of polydimethylsiloxane (PDMS) chips were synthesized, and the inorganic—organic hybrid UV absorbers were injected into its channel. These PDMS chips exhibit high transparency. When placed on the abovementioned plate under UV light irradiation, the inorganic—organic hybrid UV absorber in the channel absorbs the UV light, showing the channel patterns of the PDMS chips (Figure 6c,d).

#### CONCLUSIONS

In this work, we have successfully designed and synthesized a type of Ti-Si cross-linked inorganic-organic hybrid UV absorber coating. The hybrid UV-protective coatings overcome the disadvantages of conventional inorganic or organic UV coating with difficult synthesis methods with low transparency and poor stability. The hybrid UV absorber forms a highly efficient UV-absorbing coating at room temperature (298 K) and exhibits high transparency in the visible region and strong absorption in the UV region. These Ti-Si cross-linked inorganic-organic hybrid coatings are suitable for UV protection of heat-sensitive materials. At the same time, these UV-absorbing coatings maintain high efficiency of UV absorption even after thermal treatment at 973 K. The Ti-Si cross-linked inorganic-organic hybrid UV absorbers have the potential to expand the application of titanium-containing materials in the field of UV protection. In this way, many other UV-absorber molecules may also covalently attach to a hybrid network.

#### **■ EXPERIMENTAL SECTION**

Synthesis of a Ti-Si Cross-Linked Inorganic-Organic Hybrid UV Absorber. All the chemicals were purchased and used without further purification. UV absorbers were synthesized basically according to the following molar composition: 0.8 SiO2:0.2 TiO2:2 PEG200. The UV absorbers with titanium content between 1 and 20% were also synthesized by the same method. A certain amount of poly(ethylene glycol) (PEG200,  $M_n = 200$ , Macklin) was added to a round bottom flask. Then, tetraethyl orthosilicate (TEOS, 99.0 wt %, Aladdin) was added to the round-bottom flask and stirred at 383 K in an oil bath followed by addition of tetraethyl titanate (TEOT, 35 wt % TiO2, Aladdin). In the process of product polymerization, the byproduced ethanol was collected by a condensation tube and the temperature of the oil bath was controlled according to the rate of ethanol distillation, gradually increased to 443 K, and maintained at 443 K for 1 h. In order to promote polymerization of the product as well as accelerate the reaction, the system was vacuumed at 443 K and vacuum-treated for 1 h. After the reaction is completed, the polymerized solid product can be collected. In the process of synthesizing the UV absorber, a transesterification reaction mainly occurs and the by-product is ethanol. Through the amount of ethanol collected in the reaction process, the number of ethoxy groups in TEOS and TEOT participating in the reaction can be calculated and the degree of polymerization can be estimated.

Preparation of the Ti-Si Cross-Linked Hybrid UV-Absorbing Coatings. The Ti-Si cross-linked UV absorbers were mixed with ethanol (99.7 wt %, Aladdin). After 3 h, the UV absorbers were fully dissolved in the ethanol solution. A quartz glass was used as a coating substrate. Then, the coatings were prepared with the UV absorber solution by a spin-coating technique. The thickness of the coating was controlled by different spinning speeds. The rotational speed of an 88.0  $\mu$ m coating was 800 rpm, 1800 rpm for 15.0  $\mu$ m, 2800 rpm for 7.0  $\mu$ m, 3800 rpm for 2.0  $\mu$ m, and 5800 rpm for 0.1  $\mu$ m.

Preparation of the  $TiO_2$ -SiO\_2 Coatings. The  $TiO_2$ -SiO\_2 coatings were synthesized according to the method of previous work. An ethanolic solution of 3-glycidoxypropytrimethoxysilane (GLYMO, 98 wt %, Aladdin and the concentration is 0.37 M) and an amount of 12%  $TiCl_3$  aqueous HCl solution (Aladdin) were mixed with a molar ratio of  $SiO_2$ : $TiO_2 = 37$ . Then, an amount of propylene oxide (99.5 wt %, Aladdin; the molar ratio of propylene oxide to titanium was 5) was added to the solution. After hydrolyzing at room temperature (298 K) for 4 days. The coatings were prepared with the above solution by a spin-coating technique on the quartz slide. The obtained coatings were dried at 298 K for 1 day followed by 24 h at  $\frac{373 \text{ K}}{100}$ 

Preparation of the PDMS Chips. The PDMS chips were fabricated in polydimethylsiloxane by using a rapid prototyping technique. An SU-8-2035 photoresistor (MICROCHEM) was spin-coated onto silicon wafers and patterned by photolithography. Then, a Sylgard 184 PDMS base (Dow Coming Corporation) and a curing agent were mixed thoroughly (10:1 by mass). The samples were then degassed under vacuum and poured onto the master form. The assembly was cured in an oven (363 K, 1 h); after cooling, the devices were gently peeled from the master form and trimmed to size. Holes were punched out of the PDMS to form reservoirs for the introduction of liquid. Then, a piece of PDMS was brought into conformal contact with a quartz glass slide by irreversible bonding after oxygen plasma treatment at 363 K for 1 h.

Characterization. Solid state <sup>29</sup>Si NMR and <sup>13</sup>C NMR experiments and liquid <sup>13</sup>C NMR experiments were conducted on a Bruker Avance III spectrometer equipped with a 14.1 T and 9.4 T magnet, respectively. <sup>29</sup>Si and <sup>13</sup>C MAS NMR spectra were recorded using a high-power proton decoupling sequence with a spinning rate of 12 kHz. A total of 128 and 256 scans were accumulated with a recycle delay of 10 s for the <sup>29</sup>Si and <sup>13</sup>C MAS NMR spectra. Liquid <sup>13</sup>C NMR experiments were conducted by a one-pulse sequence with a recycle delay of 2 s and 512 scans. The transmittance spectra of the UV-protecting coatings were recorded over a range of 200 to 800 nm on a VARIAN CARY 5000. A thermogravimetric analysis (TGA) was conducted on a TA Q-600 analyzer with a heating rate of 10 K/min

from ambient temperature to 973 K in a  $\rm N_2$  flow of 100 mL/min. The thickness of the coatings was measured with a Bruker's Dektak XT Stylus Profiler System. UV light is provided by a Lumen Dynamics lamp (model: 012-64000R). Optical microscopy images were captured by a Leica S8APO stereomicroscope. Nanomechanical tests were measured by a Hysitron TI-950 Tribolndenter.

#### ASSOCIATED CONTENT

## **Solution** Supporting Information

The Supporting Information is available free of charge at https://pubs.acs.org/doi/10.1021/acsami.0c20862.

Experimental details, equation of the transesterification reaction, computational methods, NMR and FT-IR spectra, and simulated transmittance and absorbance spectra (PDF)

#### AUTHOR INFORMATION

## **Corresponding Authors**

Yunpeng Xu — National Engineering Laboratory for Methanol to Olefins, Dalian National Laboratory for Clean Energy, Dalian Institute of Chemical Physics, Chinese Academy of Sciences, Dalian 116023, China; orcid.org/0000-0002-5165-5803; Email: xuyp@dicp.ac.cn

Zhongmin Liu — National Engineering Laboratory for Methanol to Olefins, Dalian National Laboratory for Clean Energy, Dalian Institute of Chemical Physics, Chinese Academy of Sciences, Dalian 116023, China; University of Chinese Academy of Sciences, Beijing 100049, China; orcid.org/0000-0002-7999-2940; Email: liuzm@dicp.ac.cn

#### **Authors**

Jiacheng Xing — National Engineering Laboratory for Methanol to Olefins, Dalian National Laboratory for Clean Energy, Dalian Institute of Chemical Physics, Chinese Academy of Sciences, Dalian 116023, China; University of Chinese Academy of Sciences, Beijing 100049, China

Danhua Yuan — National Engineering Laboratory for Methanol to Olefins, Dalian National Laboratory for Clean Energy, Dalian Institute of Chemical Physics, Chinese Academy of Sciences, Dalian 116023, China

**Hua Xie** – National Engineering Laboratory for Methanol to Olefins, Dalian National Laboratory for Clean Energy, Dalian Institute of Chemical Physics, Chinese Academy of Sciences, Dalian 116023, China

Nan Wang — National Engineering Laboratory for Methanol to Olefins, Dalian National Laboratory for Clean Energy, Dalian Institute of Chemical Physics, Chinese Academy of Sciences, Dalian 116023, China; University of Chinese Academy of Sciences, Beijing 100049, China

Hanbang Liu – National Engineering Laboratory for Methanol to Olefins, Dalian National Laboratory for Clean Energy, Dalian Institute of Chemical Physics, Chinese Academy of Sciences, Dalian 116023, China; University of Chinese Academy of Sciences, Beijing 100049, China

Liping Yang — National Engineering Laboratory for Methanol to Olefins, Dalian National Laboratory for Clean Energy, Dalian Institute of Chemical Physics, Chinese Academy of Sciences, Dalian 116023, China; University of Chinese Academy of Sciences, Beijing 100049, China

Complete contact information is available at: https://pubs.acs.org/10.1021/acsami.0c20862

### **Author Contributions**

The manuscript was written through contributions of all authors. All authors have given approval to the final version of the manuscript. Y.X. and Z.L. conceived and guided the research project. J.X. and D.Y. designed and carried out the experiments and characterization. The coatings and PDMS chips were prepared and measured by H.X. Theoretical calculations were performed by J.X. The manuscript was drafted by J.X. and D.Y. N.W., H.L., and L.Y. took part in the discussion of experimental data and gave some suggestions.

#### Notes

The authors declare no competing financial interest.

#### ACKNOWLEDGMENTS

This research was supported by the National Key Research and Development Program of China (no. 2016YFB0301603) and the National Natural Science Foundation of China (no. 21802136). We thank Yanli He, Yijun Zheng (Dalian Institute of Chemical Physics), and Jianli Ma (Dalian University of Technology) for assistance in characterization of UV-protective coatings.

#### REFERENCES

- (1) Zayat, M.; Garcia-Parejo, P.; Levy, D. Preventing UV-light damage of light sensitive materials using a highly protective UV-absorbing coating. *Chem. Soc. Rev.* **2007**, *36*, 1270–1281.
- (2) Schultz, D. M.; Yoon, T. P. Solar Synthesis: Prospects in Visible Light Photocatalysis. *Science* **2014**, *343*, 1239176.
- (3) Zayat, M.; Pardo, R.; Castellón, E.; Torres, L.; Almendro, D.; Parejo, P. G.; Álvarez, A.; Belenguer, T.; García-Revilla, S.; Balda, R.; Fernández, J.; Levy, D. Optical and Electro-optical Materials Prepared by the Sol-Gel Method. *Adv. Mater.* **2011**, *23*, 5318–5323.
- (4) Wang, C.; Wang, D.; Dai, T.; Xu, P.; Wu, P.; Zou, Y.; Yang, P.; Hu, J.; Li, Y.; Cheng, Y. Skin Pigmentation-Inspired Polydopamine Sunscreens. *Adv. Funct. Mater.* **2018**, *28*, 18012127.
- (5) Castro Smirnov, J. R.; Calvo, M. E.; Miguez, H. Selective UV Reflecting Mirrors Based on Nanoparticle Multilayers. *Adv. Funct. Mater.* **2013**, 23, 2805–2811.
- (6) Tan, L. J.; Zhu, W.; Zhou, K. Recent Progress on Polymer Materials for Additive Manufacturing. *Adv. Funct. Mater.* **2020**, 30, 2003062
- (7) Lautenschlager, S.; Wulf, H. C.; Pittelkow, M. R. Photoprotection. *Lancet* **2007**, *370*, 528–537.
- (8) Noonan, F. P.; Recio, J. A.; Takayama, H.; Duray, P.; Anver, M. R.; Rush, W. L.; De Fabo, E. C.; Merlino, G. Neonatal sunburn and melanoma in mice Severe sunburn in newborn, but not adult, mice is linked with melanoma in later life. *Nature* **2001**, *413*, 271–272.
- (9) Deng, Y.; Ediriwickrema, A.; Yang, F.; Lewis, J.; Girardi, M.; Saltzman, W. M. A sunblock based on bioadhesive nanoparticles. *Nat. Mater.* **2015**, *14*, 1278–1285.
- (10) Sambandan, D. R.; Ratner, D. Sunscreens: an overview and update. J. Am. Acad. Dermatol. 2011, 64, 748-758.
- (11) Baker, L. A.; Marchetti, B.; Karsili, T. N. V.; Stavros, V. G.; Ashfold, M. N. R. Photoprotection: extending lessons learned from studying natural sunscreens to the design of artificial sunscreen constituents. *Chem. Soc. Rev.* **2017**, *46*, 3770–3791.
- (12) Wong, N. G. K.; Berenbeim, J. A.; Hawkridge, M.; Matthews, E.; Dessent, C. E. H. Mapping the intrinsic absorption properties and photodegradation pathways of the protonated and deprotonated forms of the sunscreen oxybenzone. *Phys. Chem. Chem. Phys.* **2019**, 21, 14311–14321.
- (13) Losantos, R.; Funes-Ardoiz, I.; Aguilera, J.; Herrera-Ceballos, E.; Garcia-Iriepa, C.; Campos, P. J.; Sampedro, D. Rational Design and Synthesis of Efficient Sunscreens To Boost the Solar Protection Factor. *Angew. Chem., Int. Ed.* **2017**, *56*, 2632–2635.

- (14) Stavros, V. G. Photochemistry: a bright future for sunscreens. *Nat. Chem.* **2014**, *6*, 955–956.
- (15) Dong, Y.; Chen, S.; Zhou, S.; Hou, S.; Lu, Q. Perspectives on the Next Generation of Sunscreen: Safe, Broadband, and Long-Term Photostability. *ACS Mater. Lett.* **2019**, *1*, 336–343.
- (16) Matta, M. K.; Florian, J.; Zusterzeel, R. Effect of Sunscreen Application on Plasma Concentration of Sunscreen Active Ingredients: A Randomized Clinical Trial. *J. Am. Med. Assoc.* **2020**, 323, 1098–1098.
- (17) Lim, J.; Sana, B.; Krishnan, R.; Seayad, J.; Ghadessy, F. J.; Jana, S.; Ramalingam, B. Laccase-Catalyzed Synthesis of Low-Molecular-Weight Lignin-Like Oligomers and their Application as UV-Blocking Materials. *Chem. Asian J.* **2018**, *13*, 284–291.
- (18) Cui, H.; Zayat, M.; Parejo, P. G.; Levy, D. Highly Efficient Inorganic Transparent UV-Protective Thin-Film Coating by Low Temperature Sol-Gel Procedure for Application on Heat-Sensitive Substrates. *Adv. Mater.* **2008**, *20*, 65–68.
- (19) Weichelt, F.; Beyer, M.; Emmler, R.; Flyunt, R.; Beyer, E.; Buchmeiser, M. Zinc Oxide Based Coatings for the UV-Protection of Wood for Outdoor Applications. *Macromol. Symp.* **2011**, 301, 23–30.
- (20) Du, Q. G.; Alagappan, G.; Dai, H.; Demir, H. V.; Yu, H. Y.; Sun, X. W.; Kam, C. H. UV-blocking ZnO nanostructure anti-reflective coatings. *Opt. Commun.* **2012**, 285, 3238–3241.
- (21) Liao, C.; Wu, Q.; Su, T.; Zhang, D.; Wu, Q.; Wang, Q. Nanocomposite gels via in situ photoinitiation and disassembly of TiO<sub>2</sub>-clay composites with polymers applied as UV protective films. ACS Appl. Mater. Interfaces 2014, 6, 1356–1360.
- (22) Jang, E.; Sridharan, K.; Park, Y. M.; Park, T. J. Eliminated Phototoxicity of  $TiO_2$  Particles by an Atomic-Layer-Deposited  $Al_2O_3$  Coating Layer for UV-Protection Applications. *Chemistry* **2016**, 22, 12022–12026.
- (23) Morimoto, T.; Tomonaga, H.; Mitani, A. Ultraviolet ray absorbing coatings on glass for automobiles. *Thin Solid Films* **1999**, 351, 61–65.
- (24) Masui, T.; Fujiwara, K.; Machida, K.; Adachi, G.; Sakata, T.; Mori, H. Characterization of Cerium(IV) oxide ultrafine particles prepared using reversed micelles. *Chem. Mater.* **1997**, *9*, 2197–2204.
- (25) Masui, T.; Yamamoto, M.; Sakata, T.; Mori, H.; Adachi, G. Synthesis of BN-coated CeO<sub>2</sub> fine powder as a new UV blocking material. *J. Mater. Chem.* **2000**, *10*, 353–357.
- (26) Assi, H.; Mouchaham, G.; Steunou, N.; Devic, T.; Serre, C. Titanium coordination compounds: from discrete metal complexes to metal-organic frameworks. *Chem. Soc. Rev.* **2017**, *46*, 3431–3452.
- (27) Zhang, J.; Li, M.; Feng, Z.; Chen, J.; Li, C. UV Raman spectroscopic study on TiO<sub>2</sub>. I. Phase transformation at the surface and in the bulk. *J. Phys. Chem. B* **2006**, *110*, 927–935.
- (28) Cohen, S.; Haham, H.; Pellach, M.; Margel, S. Design of UV-Absorbing Polypropylene Films with Polymeric Benzotriaziole Based Nano- and Microparticle Coatings. *ACS Appl. Mater. Interfaces* **2017**, *9*, 868–875.
- (29) Sirviö, J. A.; Visanko, M.; Heiskanen, J. P.; Liimatainen, H. UV-absorbing cellulose nanocrystals as functional reinforcing fillers in polymer nanocomposite films. *J. Mater. Chem. A* **2016**, *4*, 6368–6375.
- (30) Di Credico, B.; Griffini, G.; Levi, M.; Turri, S. Microencapsulation of a UV-responsive photochromic dye by means of novel UV-screening polyurea-based shells for smart coating applications. ACS Appl. Mater. Interfaces 2013, 5, 6628–6634.
- (31) Hattori, H.; Ide, Y.; Sano, T. Microporous titanate nanofibers for highly efficient UV-protective transparent coating. *J. Mater. Chem. A* **2014**, *2*, 16381–16388.
- (32) Saadat-Monfared, A.; Mohseni, M.; Tabatabaei, M. H. Polyurethane nanocomposite films containing nano-cerium oxide as UV absorber. Part 1. Static and dynamic light scattering, small angle neutron scattering and optical studies. *Colloids Surf., A* **2012**, 408, 64–70.
- (33) Mao, T.; Liu, G.; Wu, H.; Wei, Y.; Gou, Y.; Wang, J.; Tao, L. High Throughput Preparation of UV-Protective Polymers from Essential Oil Extracts via the Biginelli Reaction. *J. Am. Chem. Soc.* **2018**, *140*, 6865–6872.

- (34) Sirvio, J. A.; Visanko, M. Highly Transparent Nanocomposites Based on Poly(vinyl alcohol) and Sulfated UV-Absorbing Wood Nanofibers. *Biomacromolecules* **2019**, *20*, 2413–2420.
- (35) Han, K.; Yu, M. Study of the preparation and properties of UV-blocking fabrics of a PET/TiO<sub>2</sub> nanocomposite prepared by in situ polycondensation. *J. Appl. Polym. Sci.* **2006**, *100*, 1588–1593.
- (36) Shen, Y.; Zhu, C.; Chen, J.; Fang, Q.; Chen, W.; He, Z.; Xu, H.; Song, S. A hybrid block consisting of covalent triazine frameworks and GO aerogel with switchable selectivity between adsorption of UV filters and regeneration under sunlight. *Chem. Eng. J.* **2020**, 395, 125074.
- (37) Parejo, P. G.; Zayat, M.; Levy, D. Highly efficient UV-absorbing thin-film coatings for protection of organic materials against photodegradation. *J. Mater. Chem.* **2006**, *16*, 2165–2169.
- (38) Tolbert, S. H.; McFadden, P. D.; Loy, D. A. New Hybrid Organic/Inorganic Polysilsesquioxane-Silica Particles as Sunscreens. ACS Appl. Mater. Interfaces 2016, 8, 3160–3174.
- (39) Ortelli, S.; Poland, C. A.; Baldi, G.; Costa, A. L. Silica matrix encapsulation as a strategy to control ROS production while preserving photoreactivity in nano-TiO<sub>2</sub>. *Environ. Sci.: Nano* **2016**, 3, 602–610.
- (40) Liang, X.-Y.; Wang, L.; Wang, Y.-M.; Ding, L.-S.; Li, B.-J.; Zhang, S. UV-Blocking Coating with Self-Healing Capacity. *Macromol. Chem. Phys.* **2017**, *218*, 1700213.
- (41) Liu, F.; Liu, A.; Tao, W.; Yang, Y. Preparation of UV curable organic/inorganic hybrid coatings-a review. *Prog. Org. Coat.* **2020**, 145, 105685.
- (42) Liu, Z.; Hu, J.; Sun, Q.; Chen, L.; Feng, X.; Zhao, Y. Mussel-Inspired Multifunctional Coating for Enhancing the UV-Resistant Property of Polypropylene Fibers. *Macromol. Res.* **2017**, 25, 431–438.
- (43) Mahltig, B.; Bottcher, H.; Rauch, K.; Dieckmann, U.; Nitsche, R.; Fritz, T. Optimized UV protecting coatings by combination of organic and inorganic UV absorbers. *Thin Solid Films* **2005**, 485, 108–114
- (44) Bi, S.; Zhang, L.; Li, C. Multifunctional films with a highly oriented "nano-brick wall" structure by regulating modified TiO<sub>2</sub>@ graphene oxide/poly(vinyl alcohol) nanocomposites. *Nanoscale* **2019**, 11, 7424–7432.
- (45) Guo, H.; Klose, D.; Hou, Y.; Jeschke, G.; Burgert, I. Highly Efficient UV Protection of the Biomaterial Wood by A Transparent TiO<sub>2</sub>/Ce Xerogel. ACS Appl. Mater. Interfaces **2017**, *9*, 39040–39047.
- (46) Sun, H.; Weickert, J.; Hesse, H. C.; Schmidt-Mende, L. UV light protection through TiO<sub>2</sub> blocking layers for inverted organic solar cells. *Sol. Energy Mater. Sol. Cells* **2011**, *95*, 3450–3454.
- (47) Xu, J.; Nagasawa, H.; Kanezashi, M.; Tsuru, T. UV-Protective TiO<sub>2</sub> Thin Films with High Transparency in Visible Light Region Fabricated via Atmospheric-Pressure Plasma-Enhanced Chemical Vapor Deposition. ACS Appl. Mater. Interfaces 2018, 10, 42657—42665.
- (48) Yang, H.; Zhu, S.; Pan, N. Studying the mechanisms of titanium dioxide as ultraviolet-blocking additive for films and fabrics by an improved scheme. *J. Appl. Polym. Sci.* **2004**, *92*, 3201–3210.
- (49) Kundu, D.; Mukherjee, R. UV absorbing transparent sol-gel derived coatings on glass. *J. Mater. Sci. Lett.* **2003**, 22, 1647–1649.
- (50) Makishima, A.; Sakamoto, H.; Qiu, J. The preparation and surface roughness of CeO<sub>2</sub>-TiO<sub>2</sub> films by a sol-gel spin-coating process. *J. Non-Cryst. Solids* **2004**, 349, 355–359.
- (51) Delley, B. An all-electron numerical-method for solving the local density functional for polyatomic-molecules. *J. Chem. Phys.* **1990**, 92, 508–517.
- (52) Delley, B. From molecules to solids with the DMol(3) approach. J. Chem. Phys. 2000, 113, 7756–7764.
- (53) Jacquemin, D.; Wathelet, V.; Perpete, E. A.; Adamo, C. Extensive TD-DFT Benchmark: Singlet-Excited States of Organic Molecules. *J. Chem. Theory Comput.* **2009**, *5*, 2420–2435.
- (54) Adamo, C.; Jacquemin, D. The calculations of excited-state properties with Time-Dependent Density Functional Theory. *Chem. Soc. Rev.* **2013**, 42, 845–856.

(55) Hendon, C. H.; Tiana, D.; Fontecave, M.; Sanchez, C.; D'Arras, L.; Sassoye, C.; Rozes, L.; Mellot-Draznieks, C.; Walsh, A. Engineering the Optical Response of the Titanium-MIL-125 Metal-Organic Framework through Ligand Functionalization. *J. Am. Chem. Soc.* 2013, 135, 10942–10945.